Numerical black holes: A moving grid approach

C. Bona

Departament de Física, Universitat de les Illes Balears, E-07071 Palma de Mallorca, Spain

J. Massó*

National Center for Supercomputer Applications, 605 E. Springfield Avenue, Champaign-Urbana, Illinois 61821

J. Stela

Departament de Física, Universitat de les Illes Balears, E-07071 Palma de Mallorca, Spain

Spherically symmetric (one-dimensional) black-hole spacetimes are considered as a test for numerical relativity. A finite difference code, based in the hyperbolic structure of Einstein's equations with the harmonic slicing condition, is presented. Significant errors in the mass function are shown to arise from the steep gradient zone behind the black-hole horizon, which challenge the computational fluid dynamics numerical methods used in the code. The formalism is extended to moving numerical grids, which are adapted to follow horizon motion. The black-hole exterior region can then be modeled with higher accuracy.

PACS number(s): 04.25.Dm, 04.70.Bw

I. INTRODUCTION

Black-hole simulations are known to provide a severe test of numerical relativity, even in the one-dimensional (1D) case [1]. These strong field scenarios imply a wide dynamical range involving very different time and length scales. The coordinate degrees of freedom must be used with special care in order to prevent the numerical code from crashing when spacetime approaches a singularity. This is the idea underlying the different singularity avoiding conditions which have been proposed and tested in numerical relativity [2–4]. This approach, however, is not free from problems. Spacetime dynamics get locally frozen near the singularity, leading to an abrupt transition zone around the horizon. This can cause either steep space gradients [5] or spikes in the radial metric function [2] which make it difficult to maintain the accuracy or even lead to code crashing during numerical evolution.

A major step towards a singularity-proof scheme in numerical relativity is the use of a horizon boundary condition. The idea [6,7] is to reduce drastically the dynamical range by evolving just the observable region and imposing a suitable boundary condition on or slightly inside the horizon, which is a one-way membrane. This idea has been actually implemented in Ref. [8] by the combined use of a "horizon locking" coordinate system and a "causal" finite difference scheme which is very similar to the "causal reconnection" scheme introduced in Ref. [9]. Numerical evolution was there shown to proceed without significant errors beyond the limit of $t = 100$ m, where the previous codes that used fixed boundaries [1] became

unstable or extremely inaccurate. The results presented in Ref. [1] correspond to the maximal slicing condition [2]. This does not mean that that code could not use alternative slicings, such as the harmonic one. It is simply due to the fact that maximal slicing happens to be very robust, leading to longer numerical black-hole evolution than other singularity avoiding slicings [1].

Singularity avoidance, however, is not our only guideline in constructing a numerical relativity code. We want to use a system of evolution equations which actually translates the causal structure of the spacetime: it should be a hyperbolic system of partial differential equations with the local speed of light as characteristic speed. It has been shown recently [10,11] that the use of a harmonic time coordinate (harmonic slicing [4]) leads to such hyperbolic evolution systems, which can also be expressed in flux-conservative form. In that way, we can get the well-known structure of the hydrodynamic equations and the huge arsenal of the computational fluid dynamics (CFD) methods is at our disposal. The straightforward use of such methods has yet resulted into a 3D numerical code [12] which is able by now to evolve vacuum spacetimes admitting periodic boundary conditions.

In the present work, we will use CFD methods to improve the quality of harmonic slicing black-hole codes. The first part (Secs. II–IV) of the paper deals with the standard approach, where we use a finite difference discretization in a fixed grid. The horizon boundary condition is implemented in the second part (Secs. V–VIII) by using a moving numerical grid. The use of a moving grid is not new in numerical relativity. Wilson [13] used it to deal with the relativistic hydrodynamics equations. The same "adaptive mesh" technique was then extended to the field equations and successfully applied to the study of axisymmetric stellar collapse [14,15]. Here we provide a new application of this technique to the study of

---

*On leave of absence from Departament de Física, Universitat de les Illes Balears, E-07071 Palma de Mallorca, Spain.

black-hole evolution, where we use the grid speed to keep the numerical mesh outside the horizon. This approach is compared with the "horizon locking" condition introduced in Ref. [8].

II. THE 1D BLACK HOLE

Let us write the spherically symmetric (1D) vacuum line element in isotropic coordinates:

$$ds^2 = -\left(\frac{\rho - m/2}{\rho + m/2}\right)^2 dt^2 + \left(1 + \frac{m}{2\rho}\right)^4 (d\rho^2 + \rho^2 \, d\Omega),$$

(1)

which is locally isometric to the Schwarzschild metric. The lapse function

$$\alpha = \frac{\rho - m/2}{\rho + m/2}$$

(2)

vanishes at $\rho = m/2$, which corresponds to the black-hole horizon ($r = 2m$ in standard Schwarzschild coordinates).

The form (1) of the line element is convenient for numerical applications: (i) it is easy to express (1) in Cartesian coordinates, which allow one to consider the same problem as a test for generic (3D) numerical codes, and (ii) the metric (1) is invariant under the inversion symmetry

$$\frac{\rho}{m/2} \to \frac{m/2}{\rho}$$

(3)

mapping the black-hole outer region ($\rho > m/2$) into the inner part and vice versa; this provides a consistent inner boundary condition at the inversion point $\rho = m/2$ (the "throat"), allowing one to evolve just the exterior part of the black-hole spacetime ("wormhole" evolution: see Ref. [1]).

We shall use the space part of the line element (1) to provide the initial data for our numerical models. The singular lapse function (2) will be however replaced by a nonsingular symmetric function with initial value

$$\alpha(0, \rho) = \text{const}$$

(4)

in order to get a different spacetime slicing so that the metric components are no longer static but evolving in time. The line element is expressed in the generic spherically symmetric form

$$ds^2 = -\alpha^2(t, \rho) \, dt^2 + X^2(t, \rho) \, d\rho^2 + Y^2(t, \rho) \, d\Omega.$$

(5)

The initial condition (4) preserves the inversion symmetry (3) of the spacetime. This means that the throat connecting the two isometric sheets will remain fixed at $\rho = m/2$ and inner boundary conditions can be imposed there consistently at every step of the evolution process. Note however that the black-hole horizon [16] moves with the local light speed

$$c = \alpha/X,$$

(6)

which will be now different from zero everywhere. This means that the horizon will start moving outwards, away from the fixed throat position. The coincidence between throat and horizon in the static form (1) was because the singular lapse choice (2) caused the vanishing of the local speed of light at that point.

In order to locate the black-hole horizon [16], we will make use of the apparent horizon local definition

$$\dot{Y}/\alpha + Y'/X = 0,$$

(7)

where dots and primes stand for time and space derivatives, respectively. The mass function $M(t, \rho)$, defined by

$$2M/Y = 1 + [(\dot{Y}/\alpha)^2 - (Y'/X)^2],$$

(8)

gives at every instant the total amount of mass enclosed by a sphere of coordinate radius ρ. Of course, it does coincide with the constant parameter m in our case. Condition (7) then implies that $Y = 2m$ at the black-hole horizon.

III. THE NUMERICAL CODE

Our code is a finite difference version of Einstein field equations in first order form. This means that the set of basic quantities includes not only the lapse function α and the spatial metric components (the contravariant ones g^{ij} in our case), but also their first order space and time derivatives. The time derivative of the lapse function is given by imposing the time coordinate to be harmonic (harmonic slicing [4]). For the sake of simplicity, the remaining set of independent quantities will be described in what follows as the components of a single vector valued function $\mathbf{u}$. These quantities are taken to be independent because we consider the constraint equations as first integrals of our evolution system, which are imposed on the initial data only (free evolution approach). The conservation of the constraints can then be used as an accuracy test.

Under these conditions, it has been shown [10] that in the generic 3D case the evolution system can be written as a hyperbolic system of balance laws

$$\partial_t \mathbf{u} + \partial_k \mathbf{F}^k(\mathbf{u}) = \mathbf{S}(\mathbf{u}),$$

(9)

where the fluxes $\mathbf{F}^k$ and sources $\mathbf{S}$ are vector valued functions of $\mathbf{u}$. Moreover, it has been shown [11] that there is an infinite family of hyperbolic evolution systems which share only the physical solutions (the ones actually satisfying the constraint equations). We will use here a spherically symmetric (1D) version of one of these systems, which is explicitly given in Appendix A.

The source terms in (9) take into account the nonlinear part of Einstein's equations. We have used an operator splitting approach by considering separately the source driven evolution

$$\partial_t \mathbf{u} = \mathbf{S}(\mathbf{u})$$

(10)

and the transport process

$$\partial_t \mathbf{u} + \partial_\rho \mathbf{F}(\mathbf{u}) = 0. \qquad (11)$$

These different processes are then combined (Strang splitting [17]) to obtain a second order accurate discretization of the full equation (9).

In order to analyze the importance of the source terms in the overall evolution, we have implemented both a standard second order Runge-Kutta along with a sophisticated high order Bulirsch-Stoer method [17]. We have found that the accurate modeling of the transport step was far more significant than the source treatment in the overall evolution.

We have used a second order upwind method (see Appendix B) to deal with the transport step. Let us note that the hyperbolicity of the system (11) allows one to express it as two uncoupled subsystems with the structure of (the first order form of) the wave equation [10]. This is useful when implementing the upwind method because one can easily construct the linear combinations of the original variables which propagate along light rays going in the forward or backward direction (characteristic variables, see Appendix A).

The boundary conditions at the inner boundary are then to be imposed on the forward propagating combinations only. This is done by allowing for the inversion symmetry (3) at the throat (we will give more details in Sec. V). Conversely, the outer boundary conditions will affect only the backward propagating combinations.

IV. FIXED GRID RESULTS

We have performed our computations with an evenly spaced grid of 200 points ranging from 1 to 40 Schwarzschild radii, thus obtaining a resolution that can be tested in 3D codes [18], and allowing future comparison of results. The accuracy was monitored by computing the mass function (8), which will keep its constant value

FIG. 2. Successive plots of the time evolution of the logarithm of the metric component g_{rr}. The crosses show the successive positions of the black-hole horizon. Steep gradients appear just behind the horizon. The resulting dynamical range rises up to 80 orders of magnitude.

$M(t, \rho) = m$ only if the constraint equations are preserved. We have found that this provides an extremely sensitive error test.

The results presented in Fig. 1 actually show the mass function, as computed from the numerically evolved quantities ($m = 2$ in our case). The time values correspond to the proper time of the outermost evolving point. Errors are big around the horizon position, which is computed from (7) and marked with a cross, in spite of the huge dynamical range one gets at the black-hole throat as one approaches the singularity, as is clearly shown in Fig. 2 for the radial metric component.

This apparent paradox is explained by the collapse of the speed of light in the inner zone which locally freezes the evolution there, as is clearly shown in Fig. 3. This behavior amounts to the well known collapse of the lapse which is generic to singularity avoiding coordinate systems, like harmonic or maximal slicing. It allows us to
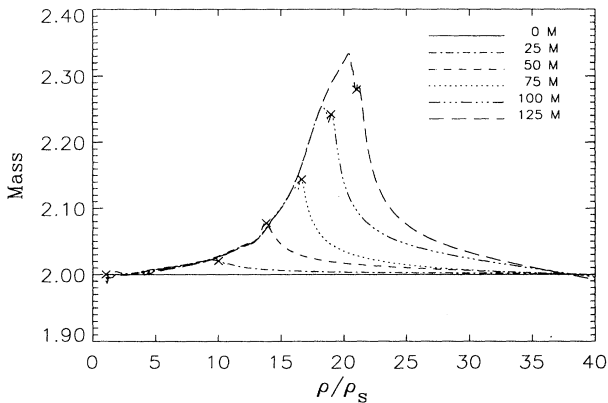

FIG. 1. Plots of the mass function (fixed grid case), which should be equal to 2 everywhere. The maximum error is around 15%. The successive horizon positions are marked with a cross. Note that the different plots coincide in the inner part, where evolution is freezing due to the light speed collapse (see Fig. 3).
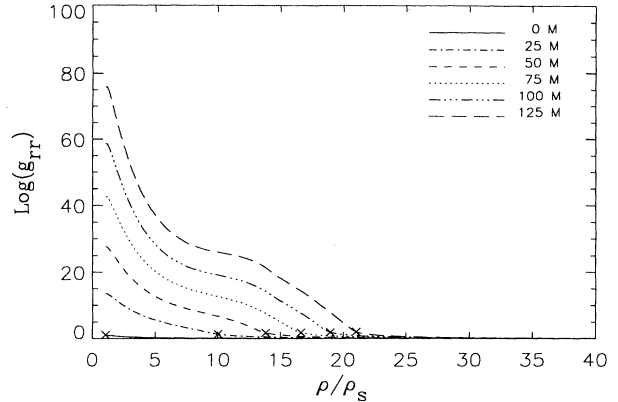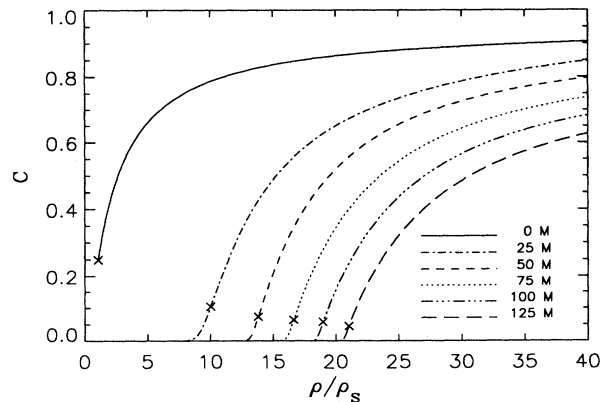

FIG. 3. Plots of the coordinate light speed, showing a sudden collapse of the inner part (the black-hole interior), due to the singularity avoidance of the harmonic slicing.

deal with the huge dynamical range in the metric components near the singularity (see Fig. 2), but it has a perverse side effect: the appearance of steep gradients near the horizon which are actually the main source of numerical errors.

One, of course, can try to reduce these errors by increasing either the grid resolution or the accuracy of the numerical method. We have rather preferred, in keeping with Ref. [8], to avoid the gradients by evolving just the exterior part of the black-hole spacetime (a moving boundary problem) with the moving grid techniques sketched in the following section.

V. A MOVING GRID APPROACH

Let us introduce a new radial function r, which is related to the previous one ρ in a time-dependent way,

$$\rho = f(t, r), \tag{12}$$

so that a grid of fixed points with respect to the new variable r will be moving with respect to the original one, attached to ρ. The first order derivatives of (12),

$$V \equiv \partial_t f, \qquad \Delta \equiv \partial_r f, \tag{13}$$

can be interpreted as the relative speed and dilation factor, respectively, as computed by an observer attached to the moving grid.

The structure of the set of conservation laws (11) does not change when written in terms of the new radial function

$$\partial_t (\Delta \mathbf{u}) + \partial_r [\mathbf{F}(\mathbf{u}) - V \mathbf{u}] = 0, \tag{14}$$

where we have transformed the quantities $\mathbf{u}$ in a scalar way. The new characteristic matrix keeps the same set of eigenvectors as the original one, so that hyperbolicity is preserved. The new characteristic speeds are obtained from the old ones simply by subtracting the grid speed V and then dividing by the dilation factor Δ. Notice that the change of variables (12) introduces just one new degree of freedom, the dilation factor being obviously related to the grid speed:

$$\partial_t \Delta - \partial_r V = 0. \tag{15}$$

Even the static choice $V = 0$ gives us the possibility of choosing a nontrivial dilation factor to deal with numerical grids which are not evenly spaced with respect to the original variable ρ. We actually used it to obtain the fixed grid results of the previous section. The reason has to do with the treatment of the inner boundary: the image under (3) of an evenly spaced set of points is no longer evenly spaced. Equation (14) with $V = 0$ provided an elegant way to preserve the overall accuracy at the inner boundary [19] without running into stability problems.

The next simplest case is the linear one, where the dilation factor depends on the time coordinate only. This leads to a linear speed profile which can be determined by the boundary values. One can apply this to the black-hole problem by demanding the grid speed to coincide with the local speed of light (characteristic speed) at the horizon. In that way, one is placing the inner boundary at the horizon (instead of at the throat), which will remain attached to a specific node of the moving grid. The profile can be fully determined by demanding the grid speed to vanish at (or near to) the external boundary. We have found this characteristic boundary approach very convenient to avoid the steep gradient zone behind the horizon while keeping a high degree of accuracy in the black-hole exterior, as we show in the following section.

VI. MOVING GRID RESULTS

We have redone with the moving grid the same computations presented in Sec. IV, under the same initial conditions. The linear relationship between the fixed and moving grid coordinates allows us to plot our moving grid results in terms of the original variable ρ, allowing a direct comparison with Sec. IV. In that sense, Fig. 4 is to be compared with Fig. 1. The successive plots start now at the horizon position because the inner part is no longer computed. Note that the error in the mass has decreased drastically: this confirms that the larger errors in Fig. 1 were due to the steep gradient zone behind the horizon.

Note that we are now placing 200 evenly spaced points in the region between the horizon and the outer boundary. The evolution can then be pursued until this region gets very small, leading to an extremely low dilation factor (extremely high characteristic speed) which freezes the evolution. In this moving grid approach, the lifetime of a numerical black hole is just the time it takes the horizon to arrive at the grid outer boundary [20].

We have also tested other initial values for the lapse function, different from (4). We found that the fixed grid code crashed in some cases, due to large errors, while the moving grid one kept its low error profile in every case. We conclude that the moving grid approach is both a more robust and a more accurate way to deal with the 1D
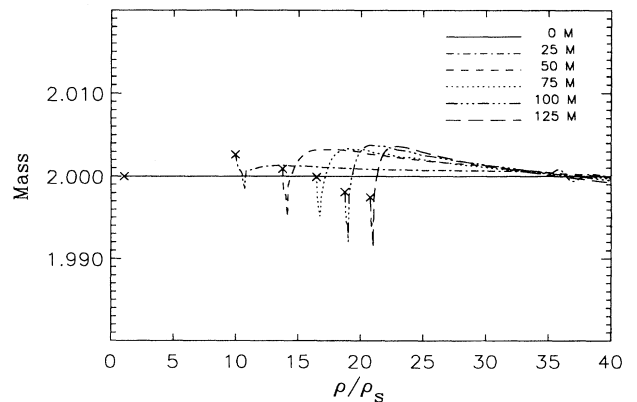

FIG. 4. Same as Fig. 1 for the moving grid case. The maximum error is now less than 0.5%. Note that the scale has been enlarged by 1 order of magnitude.

black-hole problem, significantly improving the accuracy of the results in every case.

VII. RELATED APPROACHES

A similar approach, which would be more appealing to relativists, is to consider the transformation (12) as a change of spacetime coordinates, not just affecting the grid motion, but also the metric quantities. The line element (5) would then transform into

$$ds^2 = -\alpha^2(t,r)\,dt^2 + X^2(t,r)\,(\Delta\,dr + V\,dt)^2$$
$$+Y^2(t,r)\,d\Omega^2 \tag{16}$$

so that a radial shift vector appears

$$\beta^r = V/\Delta \tag{17}$$

and the radial metric component gets multiplied by the dilation factor.

The new degree of freedom can now be used in a different way, by imposing a fixed form for the radial metric function and adding the shift β to the list of the variables [8]. The constant value of the radial metric function ensures that the use of a nonuniform dilation factor does not lead to a premature freezing of the evolution. But the main price to pay is that the structure of the original system (11) is modified at the risk of losing hyperbolicity and, with that, the possibility of applying standard numerical algorithms. We are currently studying the structure of the general 3+1 [or Arnowitt-Deser-Misner (ADM)] evolution system in order to see whether or not hyperbolicity can actually be preserved when introducing shift vectors and/or when using other algebraic gauge conditions.

There are of course other adaptive grid approaches, based on mesh refinement algorithms [21], which have been successfully applied to the 1D scalar field case [22]. Such powerful methods include sophisticated bookkeeping routines to manage the grid, putting more resolution just where it is needed, without modifying the equations in any way. The application of these methods to the generic 3D case is a big challenge to the present day computing and programming capabilities.

VIII. DISCUSSION AND OUTLOOK

We are aware that many of the difficulties one would encounter in evolving really dynamic spacetimes are avoided in the Schwarzschild test. As a first example, even in the 1D case, let us remember that a black-hole can be formed in the collapse of a supermassive star. The horizon forms at a given instant in the evolution and new horizons can appear later. The evolution of the inner boundary then will be piecewise continuous, jumping every time a new outermost horizon appears.

As stated in Sec. II, our code contains an horizon finding routine, based on the apparent horizon local definition (7), which can detect when and where a new horizon does appear. This routine can also detect whether the horizon is actually ahead of the inner boundary due to

cumulative numerical errors in computing the light speed there. We have also implemented another routine which, when the difference exceeds two grid zones, makes the inner boundary to jump from its previous location (the first grid point) to the actual horizon position, discarding the grid points between the old and new positions and recomputing the speed profile accordingly. We have found that a few of these jumps do not compromise the stability of the code and therefore we believe that the discontinuous horizon motion in 1D dynamical spacetimes can be dealt with by using the same technique.

One would encounter other difficulties when trying to extend this formalism to the multidimensional black-hole case. For instance, the horizon can expand in an anisotropic way so that the resulting speed profile can lead to a highly distorted numerical mesh. To solve this problem, one can make use of the relationship (17) between the grid speed and the shift vector. One could demand that the velocity field satisfies either the "minimal strain" or "minimal distortion" [2] or a similar condition. The corresponding set of elliptic equations should be solved by using the light speed components as inner boundary values.

But possibly the main difficulty in going to the 3D case is that the horizon finding routine cannot be a straightforward generalization of the 1D one. The multidimensional analogue of (7) contains explicitly the unit normal to the horizon surface (something one does not know *a priori*. This is the Achilles heel of 3D adaptive grid black-hole codes. We recently heard about promising progress on that subject [23,24], and it seems that it will help in solving such difficulty in a near future.

ACKNOWLEDGMENTS

APPENDIX A: EVOLUTION EQUATIONS

The set of metric variables to evolve is

$$\mathbf{u} \equiv \left(C, \Gamma_r, g^{rr}, g^{\theta\theta}, q^r{}_r, q^\theta{}_\theta, D^r{}_r, D^\theta{}_\theta\right),$$

where $C \equiv \alpha\sqrt{g^{rr}}$ is the local speed of light and we have introduced the shortcuts $D^r{}_r \equiv \partial_r \ln(g^{rr})$, $D^\theta{}_\theta \equiv \partial_r \ln(g^{\theta\theta})$, $\Gamma_r \equiv D^\theta{}_\theta - \frac{1}{2}D^r{}_r - L_r$, and $L_r \equiv \partial_r \ln(\alpha)$.

With this notation, the vacuum Einstein evolution equations in spherical symmetry can be written in first order form as

$$\partial_t C = -C^2 q^\theta{}_\theta , \tag{A1a}$$

$$\partial_t \Gamma_r = C\left[2q^\theta{}_\theta L_r + (q^\theta{}_\theta - q^r{}_r)D^\theta{}_\theta\right] , \tag{A1b}$$

$$\partial_t g^{rr} = C g^{rr} q^r{}_r \ , \tag{A1c}$$

$$\partial_t g^{\theta\theta} = C g^{\theta\theta} q^\theta{}_\theta \ , \tag{A1d}$$

$$\partial_t \left(q^r{}_r + q \right) - \partial_r \left[C (D^r{}_r + 2\Gamma_r - 2L_r) \right] \\ = C \left[(q^\theta{}_\theta)^2 - (D^\theta{}_\theta)^2 \right] \ , \tag{A1e}$$

$$\partial_t \left(q^\theta{}_\theta + q \right) - \partial_r \left[C (D^\theta{}_\theta - 2L_r) \right] \\ = C \left[q^\theta{}_\theta (2 q^\theta{}_\theta - q^r{}_r) + 2 \frac{g^{\theta\theta}}{g^{rr}} - (D^\theta{}_\theta)^2 + 2 L_r D^\theta{}_\theta \right] , \tag{A1f}$$

$$\partial_t \left(D^r{}_r - 2L_r \right) = \partial_r \left[C (q^r{}_r + q) \right] \ , \tag{A1g}$$

$$\partial_t \left(D^\theta{}_\theta - 2L_r \right) = \partial_r \left[C (q^\theta{}_\theta + q) \right] \ , \tag{A1h}$$

where we have also noted $q \equiv q^i{}_i = q^r{}_r + 2 q^\theta{}_\theta$.
The nontrivial characteristic quantities are

$$w^r_\pm = C (D^r{}_r + 2\Gamma_r - 2L_r) \pm (q^r{}_r + q) \ , \\ w^\theta_\pm = C (D^\theta{}_\theta - 2L_r) \pm (q^\theta{}_\theta + q) \ , \tag{A2}$$

with characteristic speeds $\pm C$.

APPENDIX B: DISCRETIZATION OF THE TRANSPORT PROCESS

The finite difference version of the transport equation

$$\partial_t \mathbf{u} + \partial_\rho \mathbf{F}(\mathbf{u}) = 0 \tag{B1}$$

is constructed in two steps.

In the first step, one computes all the variables at the cell interfaces (points $i \pm \frac{1}{2}$) at an intermediate time level $n + \frac{1}{2}$. The resulting predictions

$$\mathbf{u}^{n+1/2}_{i\pm1/2} \tag{B2}$$

are then used to compute the fluxes

$$\mathbf{F}^{n+1/2}_{i\pm1/2} = \mathbf{F}(\mathbf{u}^{n+1/2}_{i\pm1/2}), \tag{B3}$$

so that, in the second step, the next time level is computed in an explicit flux-conservative way:

$$\mathbf{u}^{n+1}_i = \mathbf{u}^n_i - \tfrac{dt}{dx} \left(\mathbf{F}^{n+1/2}_{i+1/2} - \mathbf{F}^{n+1/2}_{i-1/2} \right) . \tag{B4}$$

Note that the stability of this explicit scheme implies that the time interval of every step is limited by the causality condition ensuring that the characteristic speeds are lower than one grid zone per time step.

Allowing for the fact that this second step is centered both in space and in time, first order accuracy in the interface values leads to second order accuracy in the final result, because the leading error terms cancel when subtracting the fluxes between the right and left interfaces.

In order to obtain the interface values, we first compute the forward and backward first order predictions for every quantity:

$$\mathbf{u}^{FW}_{i-1/2} = \tfrac{3}{2} \mathbf{u}^n_{i-1} - \tfrac{1}{2} \mathbf{u}^n_{i-2} - \tfrac{1}{2} \tfrac{dt}{dx} \left(\mathbf{F}^n_{i-1} - \mathbf{F}^n_{i-2} \right) , \tag{B5}$$

$$\mathbf{u}^{BW}_{i-1/2} = \tfrac{3}{2} \mathbf{u}^n_i - \tfrac{1}{2} \mathbf{u}^n_{i+1} - \tfrac{1}{2} \tfrac{dt}{dx} \left(\mathbf{F}^n_{i+1} - \mathbf{F}^n_i \right) . \tag{B6}$$

Note that, when dealing with shocks or large gradients, these one-sided predictions are known to produce spurious oscillations: the predicted values at the $i - \frac{1}{2}$ interface may get out of the interval defined by the values at the grid points i and $i + 1$. This is anomalous in the sense that we are modeling a transport process and the causality condition ensures that nothing coming from outside of this interval can reach the interface at the intermediate time level. We detect this spurious behavior when one of the anomalous sequences $(u^n_i, u^n_{i+1}, u^{FW}_{i+1/2})$ or $(u^{BW}_{i+1/2}, u^n_i, u^n_{i+1})$ is monotonic. In these cases, we take $u^{FW}_{i+1/2} = u^n_{i+1}$ or $u^{BW}_{i+1/2} = u^n_i$, respectively, to make sure that our predictions do not get out of range.

We perform then a local transformation at every interface from our original quantities $\mathbf{u}$ to the set characteristic variables $\mathbf{w}$ which are given in the preceding Appendix. The hyperbolicity of our transport equations ensures that this is a one to one invertible transformation. The interface values for each characteristic component w are taken to be either the forward or backward prediction, depending on the sign of the corresponding characteristic speed (positive or negative, respectively). The interface values of the original quantities $\mathbf{u}$ are finally recovered by inverting the transformation.

[1] D. H. Bernstein, D. W. Hobill, and L. L. Smarr, in *Frontiers in Numerical Relativity*, edited by C. Evans, S. Finn, and D. Hobill (Cambridge University Press, Cambridge, England, 1989); see also D. Bernstein, Ph.D. thesis, University of Illinois at Urbana-Champaign, 1993.

[2] L. Smarr and J. York, Jr., Phys. Rev. D **17**, 1945 (1978).

[3] J. Bardeen and T. Piran, Phys. Rep. **196**, 205 (1983).

[4] C. Bona and J. Massó, Phys. Rev. D **38**, 2419 (1988).

[5] S. L. Shapiro and S. A. Teukolsky, in *Dynamical Spacetimes and Numerical Relativity*, edited by J. Cen-

trella (Cambridge University Press, Cambridge, England, 1986).

[6] W. Unruh, quoted by J. Thornburg, Class. Quantum Grav. **14**, 1119 (1987).

[7] J. Thornburgh, in Proceedings of the Toronto Meeting on Numerical Relativity, 1991 (unpublished).

[8] E. Seidel and W.-M. Suen, Phys. Rev. Lett. **69**, 1845 (1992).

[9] M. Alcubierre and B. F. Schutz, in *Approaches to Numerical Relativity*, edited by R. d'Inverno (Cambridge

University Press, Cambridge, England, 1992).

[10] C. Bona and J. Massó, Phys. Rev. Lett. **68**, 1079 (1992).

[11] C. Bona and J. Massó, Int. J. Mod. Phys. C **4**, 883 (1993).

[12] C. Bona and J. Massó, in *Approaches to Numerical Relativity* [9].

[13] J. R. Wilson, in *Sources of Gravitational Radiation*, edited by L. Smarr (Cambridge University Press, Cambridge, England, 1979).

[14] P. G. Dykema, Ph.D. thesis, University of Texas, Austin, Texas, 1980.

[15] C. Evans, in *Dynamical Spacetimes and Numerical Relativity* [5].

[16] The use of the term "black-hole horizon" is not misleading here because, in the Schwarzschild case, the event horizon and the apparent horizon do coincide.

[17] W. H. Press, B. P. Flannery, S. A. Teukolsky, and W. T. Vetterling, *Numerical Recipes* (Cambridge University Press, Cambridge, England, 1986).

[18] P. Anninos, K. Camarda, J. Massó, E. Seidel, W.-M. Suen, and J. Towns (in preparation).

[19] Note however that the resulting dilation factor is not smooth (just continuous) at the inner boundary, so that second order accuracy does not make much sense there.

[20] We can put this in the converse way: the numerical observers are falling into the static black hole and the limit is the infall time of the last observer.

[21] M. J. Berger and J. Oliger, J. Comput. Phys. **53**, 484 (1984).

[22] M. W. Choptuik, Phys. Rev. Lett. **70**, 9 (1993).

[23] P. Anninos, G. Danes, J. Massó, E. Seidel, and W. M. Suen, in *General Relativity*, edited by R. Ruffini and M. Keiser (World Scientific, Singapore, in press).

[24] J. Libson, J. Massó, E. Seidel, and W. M. Suen, in *General Relativity* [23].